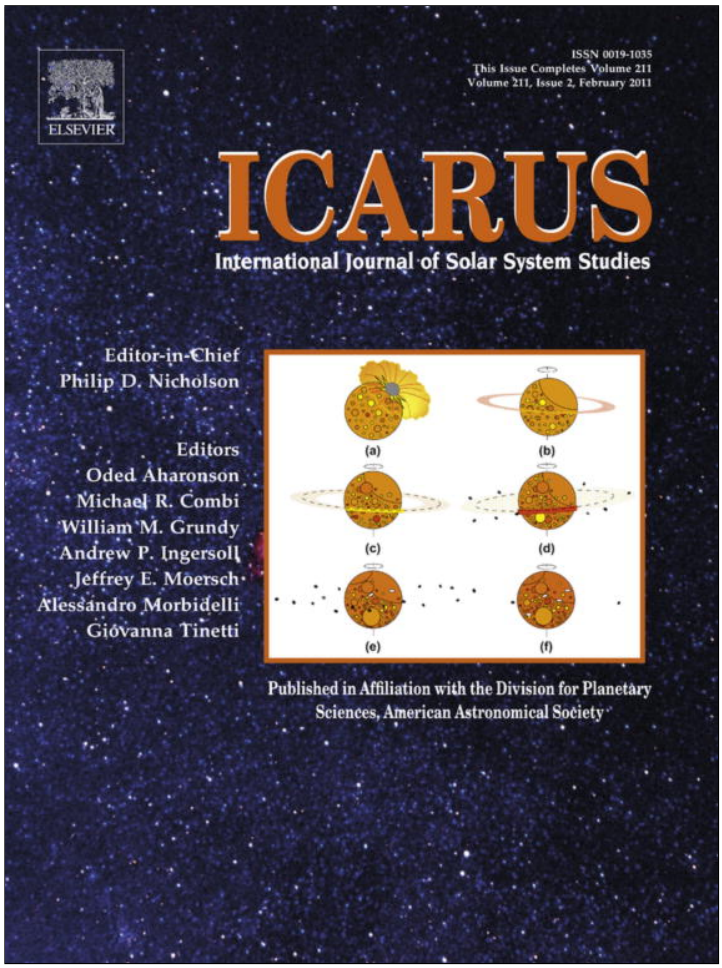

Icarus 211 (2011) 926–938

Contents lists available at ScienceDirect

Icarus

journal homepage: www.elsevier.com/locate/icarus

Persistent evidence of a jovian mass solar companion in the Oort cloud

John J. Matese *, Daniel P. Whitmire

Department of Physics, University of Louisiana at Lafayette, Lafayette, LA 70504-4210, USA

ARTICLE INFO

Article history:
Received 20 April 2010
Revised 28 October 2010
Accepted 6 November 2010
Available online 17 November 2010

Keywords:
Comets, Dynamics
Celestial mechanics
Kuiper belt
Jovian planets
Planetary dynamics

ABSTRACT

We present updated dynamical and statistical analyses of outer Oort cloud cometary evidence suggesting that the Sun has a wide-binary jovian mass companion. The results support a conjecture that there exists a companion of mass ≈1—4 $M_{Jupiter}$ orbiting in the innermost region of the outer Oort cloud. Our most restrictive prediction is that the orientation angles of the orbit plane in galactic coordinates are centered on Ω, the galactic longitude of the ascending node = 319° and i, the galactic inclination = 103° (or the opposite direction) with an uncertainty in the orbit normal direction subtending <2% of the sky. Such a companion could also have produced the detached Kuiper Belt object Sedna. If the object exists, the absence of similar evidence in the inner Oort cloud implies that common beliefs about the origin of observed inner Oort cloud comets must be reconsidered. Evidence of the putative companion would have been recorded by the Wide-field Infrared Survey Explorer (WISE) which has completed its primary mission and is continuing on secondary objectives.

1. Introduction

Anomalies in the aphelia distribution and orbital elements of outer Oort cloud (OOC) comets led to the suggestion that ≈20% of these comets were made discernable due to a weak impulse from a bound jovian mass body (Matese et al., 1999). Since that time the data base of comets has doubled. Further motivation for an updated analysis comes from the Wide-field Infrared Survey Explorer (WISE; Wright, 2007), which would have easily detected such an object orbiting in the OOC. The conjectured companion would be incapable of creating comet "storms". To help mitigate popular confusion with the Nemesis model (Whitmire and Jackson, 1984; Davis and Muller, 1984) we use the name recently suggested by Kirpatrick and Wright (2010), Tyche (the good sister of Nemesis).

In the classical view the Oort cloud (Oort, 1950) is believed to have been formed as planetesimals were scattered from the solar protoplanetary disk by the giant planets, ultimately resulting in a flattened inner Oort cloud (IOC) with a more nearly isotropic OOC. A later suggestion was that the Oort cloud instead formed by planetesimal capture from other stars when the Sun was in its initial residence in its birth cluster (Zheng et al., 1990), and the consequences of this option have recently been investigated in more detail (Levison et al., 2010). The disadvantage of the classical model of Oort cloud formation is that it predicts a scattered disk/Oort cloud population ratio of ~0.1, which is roughly a factor of 70 larger than is presently estimated (Levison et al., 2010). This problem is potentially mitigated in the birth cluster model.

The OOC was initially described as the ensemble of comets having original semimajor axes $A \geqslant 10{,}000$ AU, but today the boundary is taken to be more nearly at 20,000 AU (Kaib and Quinn, 2009). It has been shown that the majority of OOC comets that are made discernable are first-time entrants into the inner planetary region (Fernandez, 1981). The dominance of the galactic tide in making OOC comets discernable at the present epoch has been predicted on theoretical grounds (Heisler and Tremaine, 1986). Observational evidence of this dominance has been claimed to be compelling (Delsemme, 1987; Matese and Whitman, 1992; Wiegert and Tremaine, 1999; Matese and Lissauer, 2004).

Matese and Lissauer (2004) adopted an *in situ* energy distribution similar to the initial distribution of Rickman et al. (2008) and took the remaining phase space external to a "loss cylinder" (a dynamical barrier due to Saturn and Jupiter) to be uniformly populated at the present epoch. The distribution of cometary orbital elements made discernable from the tide alone was then obtained and compared with observations.

Similar modelling (Matese and Lissauer, 2002) had been performed including single stellar impulses which mapped the comet flux over a time interval of 5 Myr, in 0.1 Myr intervals. Peak impulsive enhancements ⩾20% were found to have a half-maximum duration of ≈2 Myr and occurred with a mean time interval of ≈15 Myr. Various time-varying distributions of elements were compared with the modelled tide-alone results and inferences about the signatures of a weak stellar impulse were drawn.

In Section 2 we review a discussion (Matese and Lissauer, 2004) of a subtle characteristic of galactic tidal dominance which is

* Corresponding author. Fax: +1 337 482 6699.
E-mail address: matese@louisiana.edu (J.J. Matese).

0019-1035/$ - see front matter © 2010 Elsevier Inc. All rights reserved.
doi:10.1016/j.icarus.2010.11.009

difficult to mimic with observational selection effects or bad data. Along with the more well known feature of the deficiency of major axis orientations in the direction of the galactic poles and equator, we compare with observations these predictions based on the tidal interaction alone and show that the data are of sufficiently high quality to unambiguously demonstrate the dominance of the galactic tide in making comets discernable at the present epoch. A critique of objections to this assertion (Rickman et al., 2008) is also presented. More recent detailed modelling (Kaib and Quinn, 2009) provide important insights into the evolving populations of the *in situ* and discernable populations of the Oort cloud. We comment further on these works in this section.

In Section 3 we describe the theoretical analysis combining a secular approximation for the galactic tide and for a point mass perturber, describing how a *weak* perturbation of OOC comets would manifest itself observationally. Evidence suggesting that there is such an aligned impulsive component of the OOC comet flux has been previously reported (Matese et al., 1999). It has been found that none of the known observational biases can explain the alignment found there (Horner and Evans, 2002). The size of the available data has since doubled which leads us to review the arguments here.

In Section 4 we present the supportive evidence that an impulsive enhancement in the OOC comet flux of ≈20% persists in the updated data and discuss dynamical and observational limits on parameters describing the putative companion. Also included in this section is a discussion of the lack of a corresponding signal in other comet data. Section 5 summarizes our results and presents our conclusions.

2. Secular dynamics of the galactic tide

Near-parabolic comets are most likely to have their perihelia reduced to the discernable region. The dynamics of the galactic tide acting on near-parabolic OOC comets is most simply described in a Newtonian framework (Matese et al., 1999; Matese and Lissauer, 2002, 2004). A summary of their analyses is now given and followed with the evidence that the galactic tidal perturbation dominates in making OOC comets discernable at the present epoch.

2.1. Theory

Saturn and Jupiter provide an effective dynamical barrier to the migration of OOC comet perihelia. OOC comets that are approaching the planetary zone at the present time were unlikely to have had a prior perihelion, q_{prior}, that was interior to the "loss cylinder" radius, $q_{lc} \approx 15$ AU, when it left the planetary region on the present orbit. The simplifying assumption $q_{lc} \leqslant q_{prior}$ is then made for the present orbit. During the present orbit comet perihelion will then have been changed by the galactic tide (and by any conjectured companion or stellar perturbation). The orbital elements just before re-entering the planetary region on the present orbit are commonly referred to as "original" and will be, in essence, the observed values with the exception of the semimajor axis (perturbations by the major planets do not significantly change any other orbital element of OOC comets). Thus q_{prior} is changed to $q_{original} \approx q_{obs}$, the observed value, during the course of the present orbit. As an observed comet comes within a discernable region ($q_{obs} \leqslant q_{discernable} \approx 5$ AU) and leaves the planetary region again, the semimajor axis will have been changed from $A_{original}$ to A_{future}, i.e., $A_{future} \equiv A_{prior}$ for the *next* orbit. This "daughter" comet is most likely ejected or turned into a comet in the IOC with a small fraction returning to the OOC. Daughter comets returning to the discernable zone may fade and be more difficult to observe (Wiegert and Tremaine, 1999), but constitute one potential source of observed IOC comets. The 17th Catalogue of Cometary Orbits (Marsden and Williams, 2008) indicates that ≈10% of observed original OOC comets exit the planetary region as future OOC comets. Therefore the population of observed OOC comets should be dominated by first-time entrants to the loss cylinder. In the following we adopt the notation $A \equiv A_{original}$.

For near-parabolic comets, the angular momentum per unit mass determines the perihelion distance, $\mathbf{H} \equiv \mathbf{R} \times \dot{\mathbf{R}}$, ($\mathbf{H} \perp \mathbf{q}, H \approx \sqrt{2\mu_\odot q}$). With these assumptions, an OOC comet entering the loss cylinder region for the first time had perihelion distances $q_{obs} \leqslant q_{discernable} < q_{lc} \leqslant q_{prior}$. Therefore, reducing q in a single orbit requires a decrease in angular momentum from the galactic tidal torque (and/or from angular momentum changes by the putative companion or star),

$$\Delta\mathbf{H} \equiv \mathbf{H_{obs}} - \mathbf{H_{prior}}, \quad \text{or}$$
$$q_{prior} - q_{obs} = \left(\Delta\mathbf{H}^2 - 2\mathbf{H_{obs}} \cdot \Delta\mathbf{H}\right)/2\mu_\odot. \tag{1}$$

The weakest perturbation that could make a comet discernable would reduce the prior perihelion distance from $q_{prior} \approx q_{lc}$ to $q_{obs} \approx q_{discernable}$ (see Fig. 1) such that

$$|\Delta\mathbf{H}|_{min} = \sqrt{2\mu_\odot q_{lc}} - \sqrt{2\mu_\odot q_{discernable}}. \tag{2}$$

Also of interest is the evolution of the aphelion orientation, $\hat{\mathbf{Q}} \equiv (\cos B \cos L, \cos B \sin L, \sin B)$, expressed in terms of the aphelion latitude, B, and longitude, L.

If the galactic tide dominates in making OOC comets discernable Eq. (1) implies that for *weak* perturbations, the tidal characteristic, $S \equiv \mathrm{Sign}(\mathbf{H_{obs}} \cdot \Delta\mathbf{H_{tide}})$ will more often be −1 than +1. Detailed modelling results (Matese and Lissauer, 2004) confirm this implication. This characteristic combination of observed orbital elements forms an *essential aspect of the present analysis* and has

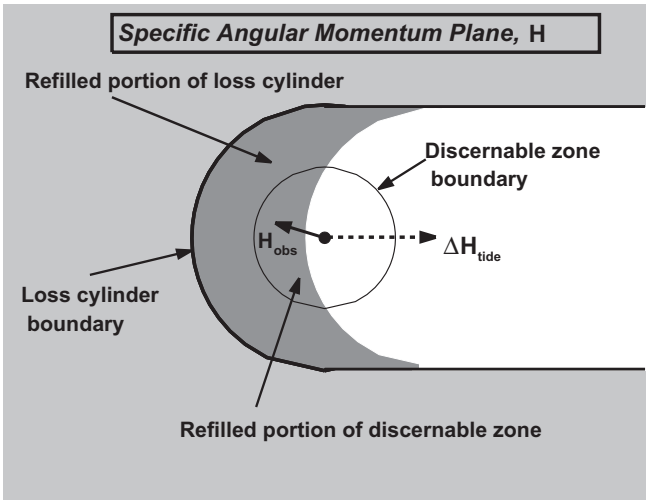

Fig. 1. Schematic illustration of the plane of specific angular momentum phase space, **H**, for a given A and $\hat{Q}$, the aphelion direction defining the normal to this plane. Phase space points illustrated have the *same* values of A, B, and L, but cover the entire region of **H** just outside the loss cylinder. Light gray shaded region outside the loss cylinder boundary ($H > H_{lc} \propto \sqrt{q_{lc}}$) denotes the filled phase space of comets leaving the planetary region on their prior orbits. The uniform displacement of all phase space points one orbit later by a tidal perturbation $\Delta\mathbf{H_{tide}}$ is shown partially refilling the loss cylinder region (indicated as the dark gray region). The discernable zone within the loss cylinder ($H < H_{discernable} \propto \sqrt{q_{discernable}}$) is indicated. It remains unfilled for negligible perturbations of small-A (IOC) comets, becomes totally refilled for strong perturbations of large-A OOC comets, and, as illustrated here, is partially refilled for weak perturbations of intermediate-A OOC comets. The tidal characteristic $S \equiv \mathrm{Sign}(\mathbf{H_{obs}} \cdot \Delta\mathbf{H_{tide}}) = -1$ for all *observed* comets in the refilled portion of the discernable phase space here. Over successive orbits a shadow region of unfilled phase space (shaded white) will be formed for IOC and intermediate-A OOC comets.

not been included in modelling results presented elsewhere (e.g., Rickman et al., 2008; Kaib and Quinn, 2009).

A graphical illustration of this theme in Fig. 1 shows the phase space changes in **H** for a specific choice of $\hat{\mathbf{Q}}$ and A over the course of a single orbit period. As comets recede from the planetary region on their prior orbits, the interior of the loss cylinder phase space region is essentially emptied of OOC comets by planetary perturbations. The adjacent exterior region remains uniformly populated in this model. To lowest order in q/A, i.e., the near-parabolic phase space region just outside the loss cylinder boundary, the vector displacement in specific angular momentum, $\Delta\mathbf{H}_{\mathbf{tide}}$, is independent of the prior value of angular momentum, $\mathbf{H}_{\mathbf{prior}}$, and depends only on A and the major axis orientation, $\hat{\mathbf{Q}}$, which are taken to be fixed for the phase space of Fig. 1. In a single orbit all nearby specific angular momentum phase space points, filled and empty, are displaced uniformly (Matese and Lissauer, 2004). Fig. 1 illustrates that in the present modelling, the phrase "loss cylinder" which is used to describe the Saturn–Jupiter dynamical barrier might be more appropriately changed to "loss circle".

The magnitude of the single-orbit angular momentum displacement is strongly dependent on A, varying as $A^{7/2}$. Small-A comets are defined here as IOC comets having galactic perturbations $<|\Delta\mathbf{H}|_{min}$, unable to repopulate the discernable zone. Large-A OOC comets are defined here as those having strong tidal perturbations resulting in large displacements in **H** that completely refill the discernable zone, making $S = \mp 1$ equally likely. Intermediate-A OOC comets are defined here as those that are weakly perturbed by the tide and only partially refill the discernable zone. Intermediate-A comets preferentially have $S = -1$, as seen in Fig. 1. In this context intermediate-A OOC comets have the smallest *observed* values of A among OOC comets if the tide dominates in making comets discernable. The fuzzy boundaries between small-A, intermediate-A and large-A depend weakly on B and L. We choose the boundaries for these intervals based on data discussed in Section 3.

Therefore, *independent of stellar influences on the in situ distribution of semimajor axes*, if the galactic tidal interaction with the OOC dominates impulsive interactions in producing discernable OOC comets at the present epoch we should see

- a preponderance of OOC comets with $S = -1$ over those with $S = +1$, and
- an association in which $S = -1$ correlates with the smallest observed values of A for OOC comets.

Conversely, if perturber impulses dominate in producing OOC comets at the present epoch, the unique tidal characteristic S should be a random variable and should be uncorrelated with A.

2.2. Observational evidence for tidal dominance at the present epoch

Our data are taken from the 17th Catalogue of Cometary Orbits from which we convert the ecliptic Eulerian orbital angles into the galactic angles B, L and α, the orientation angle of **H** defined in Matese and Lissauer (2004). The Catalogue lists 102 comets with $A > 10^4$ AU (see Appendix B) of the highest quality class, 1A (we count the split comet C/1996-J1A(B) as a single comet). The quality class predominantly distinguishes the accuracy of the original semimajor axis determination (Marsden et al., 1978). Since our analysis depends sensitively on an accurate determination of A, we restrict our detailed discussions to class 1A comets. In a previous analysis (Matese et al., 1999) the orbital elements of 82 comets of quality classes 1A + 1B with $A > 10^4$ AU given in the 11th Catalogue were used, 47 of which were class 1A. In the following all references to Catalogue data will be to class 1A comets unless otherwise specified.

The first observational indication that the galactic tide dominates involved the distribution in the galactic latitude of aphelion, B (Delsemme, 1987). One finds (Matese et al., 1999) that the dominant disk tidal term in the perturbation is $\propto|\sin B\cos B|$ (Rickman et al. (2008) conclude that this perturbation is $\propto|\sin B|$ rather than $\propto|\sin B\cos B|$). B and L are sensibly constant in the course of a single orbit since **Q** has significant inertia for near-parabolic orbits. Therefore, if the tide dominates we should expect deficiencies of major axis orientations along the galactic poles and the galactic equator, and peaks near $B = \pm 45°$. One might argue that observational selection effects can artificially produce an equatorial gap, but polar gaps will be more difficult to attribute to an observational selection effect.

In Fig. 2 we show the results presented as a distribution in $|\sin B|$, which would be uniform for a random distribution. Polar and equatorial gaps are clear, as predicted if the galactic tide dominates. A small (but potentially informative) discrepancy is the location of the peak. If the tide dominates, our modelling (Matese and Lissauer, 2004) predicts a peak at $|\sin B| \approx 0.7$, somewhat larger than seen in the data. We now look to the tidal characteristic S to further emphasize tidal dominance.

The prediction that $S = \mp 1$ should be equally likely for large-A OOC comets, and that there should be a preponderance of $S = -1$ for intermediate-A OOC comets (see Fig. 1) is now considered. In terms of the original orbital binding energy parameter $x \equiv 10^6$ AU/A, class 1A comets have a mean formal error of $\approx$5 units, but the uncertainty due to unmodelled outgassing effects is likely to be somewhat larger (Kresák, 1992; Królikowska, 2006). In particular the fraction of nominally unbound original orbits listed in Appendix B (7 of 102) is likely indicative of the true errors embodied in the tails of the class 1A OOC comet energy distribution. For comparison, class 1B comets nominally have a mean formal error of $\approx$12 units but the fraction of unbound original orbits with $x < 100$ is 13 of 51 suggesting that the nominal uncertainty understates the true uncertainty much more than for class 1A comets.

In Fig. 3 we show the cumulative binding energy distribution of 66 comets with $S = -1$ and 36 comets with $S = +1$. The binomial probability that as many or more would exhibit this imbalance if in fact $S = \mp 1$ were equally likely is 2×10^{-3}. Further, as predicted by tidal dynamics, this preponderance of $S = -1$ also correlates with intermediate-A OOC comets in a statistically significant manner. $S = \mp 1$ is approximately equally likely for comets with $x \leqslant 30$, suggesting that for this range of semimajor axes the galactic tide is strong enough to refill the discernable zone almost completely, i.e., the tidal efficiency is nearly 100% (Matese and Lissauer, 2002). We therefore take this as the observationally defined boundary between large-A and intermediate-A OOC comets. In contrast, for $30 < x < 100$ the evidence is that the tide weakens dramatically since 45 comets have $S = -1$ and only 12 have $S = +1$. The binomial

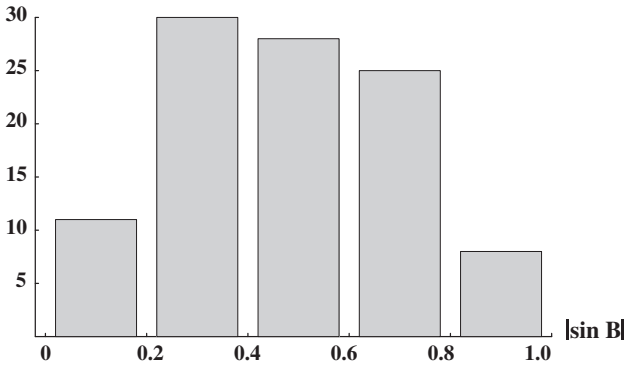

Fig. 2. The distribution in $|\sin B|$ for comets listed in Appendix B.

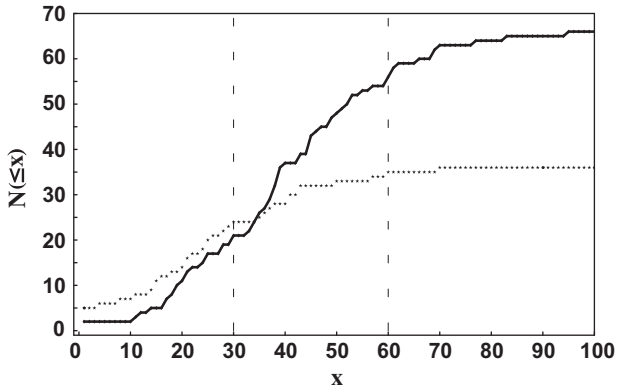

Fig. 3. The cumulative binding energy distribution ($x \equiv 10^6$ AU/A) for comets listed in Appendix B, separately illustrated for $S = \mp 1$. Solid line $\leftrightarrow S = -1$, dotted line $\leftrightarrow S = +1$.

probability that as many or more would exhibit this imbalance if in fact $S = \mp 1$ were equally likely for this energy range is 7×10^{-6}. This is unambiguous evidence that the class 1A OOC comet data are of sufficiently high quality and sufficiently free of observational selection effects to detect this unique imprint of tidal dominance in producing discernable OOC comets at the present epoch.

Kaib and Quinn (2009) have found that ≈5% of comets that are discernable for the first time should have $60 < x$, the majority of which have evolved from a primordial location in the IOC. It is unlikely that these comets have had their prior orbit perihelia outside the loss cylinder and therefore would not satisfy $|\Delta\mathbf{H}| > |\Delta\mathbf{H}|_{min}$. Taking account of expected errors in the binding energies we adopt $30 < x < 60$ as the defining interval for intermediate-A OOC comets and $60 \leqslant x$ as our working definition for the IOC. Discernable OOC comets with nominal original energies $-\infty < x < 60$ will be referred to as *new* comets as they are likely to be first-time entrants into the discernable zone. Discernable IOC comets with $60 \leqslant x \leqslant 1000$ will be referred to as *young* comets.

These clear signatures of galactic tidal dominance in making OOC comets discernable do not mean that we must abandon hope for detecting any impulsive imprint on the distributions, as we describe in Section 3.

2.3. Comparisons with recent modelling

Kaib and Quinn (2009) have done the most complete modelling of the production of discernable long-period comets (LPC) from the Oort cloud in an attempt to infer the Sun's birth environment. They closely follow whether a new comet was born in the OOC or in the IOC and find that roughly comparable numbers of each primordial population are made discernable after a suitable time lapse. The binding energy distribution for the two populations (their Fig. S4) differs in that the distribution for comets born in the IOC peaks at $x \approx 38$ while that for comets born in the OOC peaks at $x \approx 28$. They conclude that the IOC pathway provides "an important, if not dominant, source of known LPCs". The primordial origin of discernable comets is not important in our loss-cylinder modelling.

Very few observed comets with $30 < x < 60$ are likely to have had prior perihelia within the loss cylinder. We have used their Fig. S4 as a guide to the energy range most likely to show evidence of a weak impulsive component of the observed OOC.

Rickman et al. (2008) have also embarked on an ambitious modelling program of the long term evolution of the Oort cloud which emphasizes a fundamental role for stellar perturbations. They demonstrate that over long timescales stellar impulses are needed to replenish the phase space of the OOC which is capable of being made discernable by the galactic tide. Massive star impulses serve to efficiently refill this feeding zone for a period of several 100 Myr and therefore provide one aspect of the synergy with the galactic tide that make these comets discernable.

They also assert that "treating comet injections from the Oort cloud in the contemporary Solar System as a result of the galactic tide alone is not a viable idea". This statement follows from their observations that a tide-alone model *evolving over the lifetime of the Solar System* differs significantly at the present epoch from a combined impulse-tide model.

But their modelling does not shed light on the question of the dominant dynamical mechanism responsible for injecting OOC comets into the inner planetary region *at the present epoch*. Their work makes detailed predictions using results averaged over 170 Myr. Such a large time window inevitably includes many individual stellar perturbations which contribute directly to the time-averaged flux. Separating out the dominant perturbation making these comets discernable at the present epoch would be best obtained if they (i) "turn off" both perturbations at the present epoch, (ii) wait for the discerned flux to dissipate, and then (iii) alternately determine subsequent distributions produced by each perturbation separately turned on. This analysis was not performed.

Indeed, one can compare our predictions (Matese and Lissauer, 2004) for discernable distributions in A and the A-dependent discernable zone refill efficiency with Rickman et al. (2008) (where they use the term "filling factor" in the same context as our "efficiency"). The tide-alone results *at the beginning* of their simulations (see their Fig. 7 and Table III) provide the most appropriate comparison since their phase space then is most nearly randomized and comparable to that used in our previous work. One finds that these two sets of distributions are in good agreement.

Their combined modelling of the latitude distributions does predict a peak at $|\sin B| \approx 0.5$, more nearly in agreement with observations shown in Fig. 2 (however they assert that their predictions do not agree with observations without any discussion of the nature of the discrepancies perceived). If this difference with our tidal model prediction of a peak at $|\sin B| \approx 0.7$ is supported in the future it may provide evidence that the *in situ* phase space refilling of the OOC by stellar perturbations is indeed detectably incomplete at the present epoch, a point emphasized by them. This would not contradict our assertion that the unambiguous evidence is that the galactic tide dominates in making OOC comets discernable at the present epoch. It remains for them to demonstrate that the modelling adopted here (Matese and Lissauer, 2002, 2004) is no longer viable in describing observations at the present epoch. We conclude our remarks by noting that neither of the above analyses have tracked the orbital characteristic S in the production of new comets, a major measure of galactic dominance in our work.

3. Dynamics of a weak impulsive perturbation

3.1. Theory

The dynamics of a weak perturbation of a near-parabolic comet by a solar companion or field object is now considered. The change in the comet's specific heliocentric angular momentum induced by a perturber is given by

$$\dot{\mathbf{H}}_{\mathbf{pert}} = \mu_p(\mathbf{R} \times \mathbf{r})\left(\frac{1}{|\mathbf{R} - \mathbf{r}|^3} - \frac{1}{r^3}\right), \tag{3}$$

where $\mu_p = GM_p$ and M_p is the perturber mass located at heliocentric position $\mathbf{r}$ and $\mathbf{R}$ is the heliocentric comet position. In terms of the perturber true anomaly, f, we have $r = p/(1 + e_p\cos f)$, with $p = a(1 - e_p{}^2)$. We then obtain for near-parabolic comets

$$\frac{d\mathbf{H}_{\mathbf{pert}}}{df} = \sqrt{\mu_\odot a}\frac{\mu_p}{\mu_\odot}\left(\widehat{\mathbf{Q}}\times\hat{\mathbf{r}}\right)\frac{R}{b}\left(\frac{r^3}{|\mathbf{R}-\mathbf{r}|^3}-1\right), \tag{4}$$

where $b = a\sqrt{1-e_p^2}$, the semiminor axis of the perturber. One then constructs

$$\Delta\mathbf{H}_{\mathbf{pert}} = \sqrt{\mu_\odot a}\frac{\mu_p}{\mu_\odot}\widehat{\mathbf{Q}}\times\mathbf{I}, \tag{5}$$

where the dimensionless integral $\mathbf{I}$ is taken around an interval of the perturber true anomaly $\Delta f \equiv f_o - f_i$ that corresponds to the comet orbital time interval between $t_o \equiv 0$, the present epoch, and $t_i \equiv -2\pi\sqrt{A^3/\mu_\odot}$,

$$\mathbf{I} \equiv \int_{f_i}^{f_o} df\hat{\mathbf{r}}\frac{R}{b}\left(\frac{r^3}{|\mathbf{R}-\mathbf{r}|^3}-1\right). \tag{6}$$

The first term in $\mathbf{I}$ corresponds to the perturber interaction with the comet, the second with the Sun. For a specified perturber orbital ellipse, $\mathbf{I}$ is determined by the cometary $\widehat{\mathbf{Q}}$ and A as well as the companion's present value of the true anomaly, f_o. Eq. (3) is more convenient to use in an impulse approximation as has been done in a previous analysis of the combined tide-stellar impulse interaction with the OOC (Matese and Lissauer, 2002). Eq. (4) is more appropriate if one wishes to include the slow "reflex" effects of a bound perturber on the Sun.

3.2. Combined tidal and impulsive interaction

The galactic tidal perturbation and any putative point source perturbation of the Sun/OOC are, in nature, superposed in the course of a cometary orbit. For weak perturbations the two effects can be superposed in a vector sense, $\mathbf{H}_{\mathbf{obs}} \equiv \mathbf{H}_{\mathbf{prior}} + \Delta\mathbf{H}_{\mathbf{pert}} + \Delta\mathbf{H}_{\mathbf{tide}} \equiv \mathbf{H}_{\mathbf{prior}} + \Delta\mathbf{H}_{\mathbf{net}}$. The cometary phase space of comets will have the prior loss cylinder distribution displaced by $\Delta H_{\mathbf{net}}$. The standard step function for the prior distribution of angular momentum is changed to a uniformly displaced distribution, similar to that illustrated in Fig. 1, but with $\Delta\mathbf{H}_{\mathbf{tide}}$ replaced by $\Delta\mathbf{H}_{\mathbf{net}}$, $q_{prior} - q_{obs} = (\Delta\mathbf{H}_{\mathbf{net}}^2 - 2\mathbf{H}_{\mathbf{obs}}\cdot\Delta\mathbf{H}_{\mathbf{net}})/2\mu_\odot$.

3.3. Weak impulsive effects on the discernable energy and spatial distributions

Matese and Lissauer (2002) modelled the time-dependent changes in new comet orbital element distributions that resulted from a *weak stellar impulse*. In particular, the *in situ* energy distribution was taken to be essentially unchanged, as described above. The number of comets in the large-A ($x \leqslant 30$) interval that became discernable after an impulse was found to be essentially unchanged from the case with no impulse, although the specific comets made discernable were changed. That is, the ≈100% efficiency of refilling the discernable zone remains ≈100% throughout the stellar impulse for large-A comets. This can be visualized in Fig. 1 when we consider a large $\Delta\mathbf{H}_{\mathbf{tide}}$ that completely refills the loss cylinder and the comparative case where the large $\Delta\mathbf{H}_{\mathbf{tide}}$ is modified by a weak $\Delta\mathbf{H}_{\mathbf{pert}}$. Independent of whether the impulse slightly increased or decreased the perturbation, a large $|\Delta\mathbf{H}_{\mathbf{net}}|$ will still tend to completely refill the loss cylinder, albeit with different comets.

For the intermediate-A population the discussion is more subtle. Suppose that for a specific $\widehat{\mathbf{Q}}$ a comet population with $x \approx 35$ will partially fill the discernable zone due to the tide (see Fig. 1). If some of those comets experience an impulse that increases $|\Delta\mathbf{H}_{\mathbf{net}}|$, the discernable zone will be more completely filled. However other comets will be impulsed such that $|\Delta\mathbf{H}_{\mathbf{net}}|$ is *decreased*. This will in turn decrease the number of discernable comets for this value of x leaving the efficiency for this x only moderately increased.

Consider now the case for a population with $x \approx 45$. The tidal perturbation will be smaller by a factor of ≈0.4 from the $x \approx 35$ population, which may be inadequate to make any of these comets discernable in our loss cylinder model. In this case an impulsive torque preferentially opposed to the tidal torque will have no effect on the number of observed comets for this x since none would have been observed in its absence. But for those comets which have a weak impulsive torque preferentially aiding the tide, some will be made discernable that would not have been in the absence of an impulse. Therefore the efficiency for this x will increase from zero, and it will preferentially have $S = -1$. The net effect for a weak impulse is to create an enhanced observed OOC comet population along the track of the perturber that preferentially has intermediate-A and $S = -1$. These features have been demonstrated in detailed modelling for a *weak stellar impulse* (Matese and Lissauer, 2002). Rickman et al. (2008) also discuss in detail this aspect of synergy but do not consider the importance of the characteristic, S, in this discussion.

In reality, the step function distribution of prior orbits for OOC comets used in the loss cylinder model is a crude first approximation. A small fraction of new comet orbits recede from the planetary region as future new comets with perihelia *inside* the loss cylinder. This does not obviate the arguments invoked above. Along with the original energy errors associated with observational uncertainties and outgassing effects, we can understand why the observed spread in original OOC energies seen in Fig. 3 is somewhat larger than predicted in our loss cylinder model and is consistent with more realistic modelling (Kaib and Quinn, 2009).

4. Observational evidence for an impulse

Matese et al. (1999) noted an excess of new comet major axes along a great circle roughly centered on the galactic longitudinal bins 135° and 315° using 11th Catalogue data of quality classes 1A + 1B with $x < 100$. Further, they found that the excess was predominantly in the intermediate-A OOC population and had a larger proportion of $S = -1$, consistent with it being impulsively produced. In Fig. 4 we now display the distribution of the aphelia longitudes for comets in Appendix B. We see that the excess remains in the present data.

4.1. Monte Carlo simulations

There is no obvious *a priori* reason why a systematic explanation of the overpopulation should be associated with a plane passing through the galactic poles. Further, choosing longitude bins for comparison has an obvious bias in that it preferentially excludes

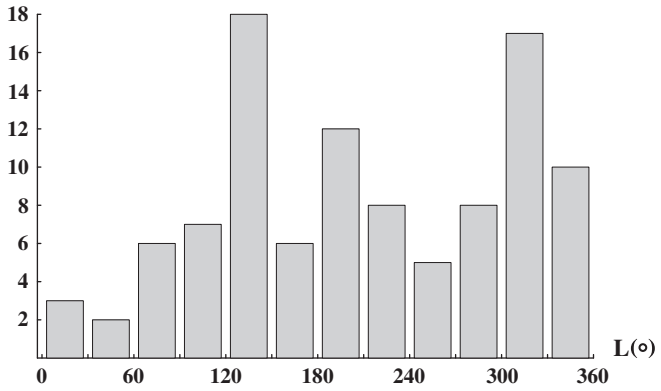

Fig. 4. The distribution of aphelia longitude, L, for comets listed in Appendix B.

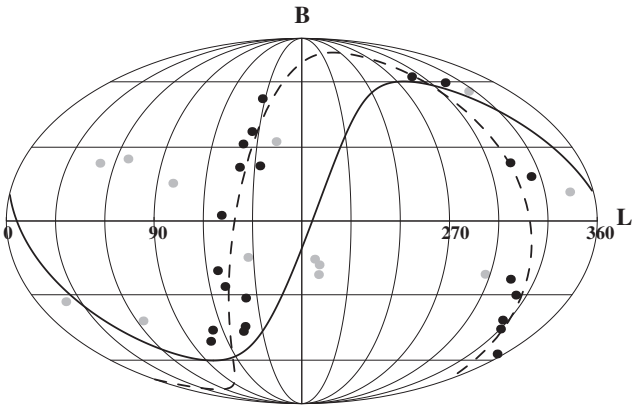

Fig. 5. The scatter distribution for aphelia directions of 17th Catalogue new comets having a binding energy parameter, $x \equiv 10^6$ AU/A, in the interval $30 < x < 60$ and tidal characteristic $S = -1$. Solid curve: ecliptic plane. Dashed curve: maximum likelihood plane with $i = 103°$, $\Omega = 319°$. Black dots: aphelia directions within a band of width ±9.6° covering 1/6 of the celestial sphere and centered on the maximum likelihood great circle path. Gray dots: exterior to the band.

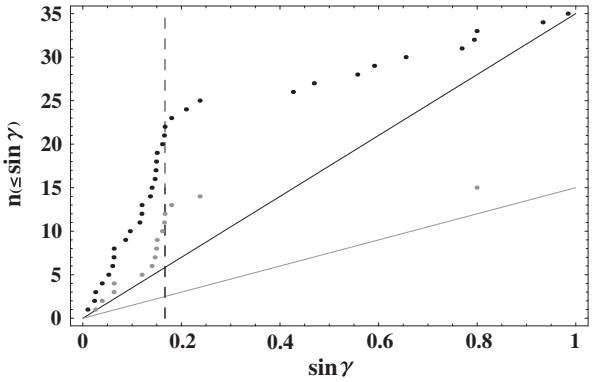

Fig. 7. The cumulative distribution of the number of major axes of new comets having $30 < x < 60$ and $S = -1$ that fall within an annular band of solid angle $4\pi \sin\gamma$ centered on the maximum likelihood great circle $i = 103°$, $\Omega = 319°$. Black: 17th Catalogue data. Gray: 11th Catalogue data. Solid lines are for random distributions. Dashed line indicates annular band of maximum likelihood width ±9.6° which includes $\Gamma = 1/6$ of the celestial sphere.

solid angles near the poles where the tide is weak. We therefore consider great circle fits that count the number of major axes within an annular band of width ±9.6°, which has the same solid angle, $4\pi/6$, as the two overpopulated aphelia longitude bins in Fig. 4. The data that we now analyze includes comets listed in Appendix B which are intermediate-A OOC comets, $30 < x < 60$, with $S = -1$. As described above, this is the subset most likely to exhibit evidence of a weak impulsive component. Of these 35 comets, 15 were included in the 11th Catalogue considered by Matese et al. (1999). In Fig. 5 we show the aphelia scatter of this data.

We now consider the null hypothesis, $\mathscr{H}_\circ$, that the dominant galactic tide can explain the pattern of major axis orientations of this data subset and that the observed longitudinal asymmetry is due to chance alone and not due to a systematic cause. Separately investigated are the original 11th Catalogue, the present 17th Catalogue and the data formed from their difference.

For each of these we perform a variation of the Monte Carlo simulation done elsewhere (Horner and Evans, 2002) which considered the original conjecture. Each comet in the data maintains its measured value of B, but is randomly assigned a value for L. This simulation choice is suited to the null hypothesis that the galactic tide acts alone, producing minima in the number of major axes at the galactic poles and equator and a near-uniform distribution in aphelia longitudes. An analysis is performed for the simulation to find the orientation of the great circle band orbit normal $\hat{\mathbf{h}}$ of half-width $\Gamma \equiv \sin 9.6° = 1/6$ which maximizes the number of simulated major axes interior to the band. Counting is done for *all* possible great circle orientations with normal directions $\hat{\mathbf{h}}$ stepped in a grid covering solid angles $(1°)^2$. Great circle orientations are denoted by the galactic longitude of ascending node, Ω, and the galactic inclination, i. The same results are obtained for opposite great circle normal vectors $-\hat{\mathbf{h}} \leftrightarrow (\Omega - 180°, 180° - i)$.

We then record that maximal number, κ. Repeating the process 10^4 times we find the conditional distribution f_κ (keeping the latitudes fixed and assuming the null hypothesis is correct) as estimated by the Monte Carlo simulation. The process is repeated for the 11th Catalogue data which includes $n = 15$ axes, the complete 17th Catalogue data which includes $n = 35$ axes, as well as for the 17–11th Catalogue subset. A summary of results is given in Table 1 for each set of evidence $\mathscr{E}$. As an example, for the 11th Catalogue data the Monte Carlo simulations estimate that in only 3 of 10^4 cases would we find as many as 12 major axes in the band if in fact the null hypothesis was correct. When we repeat the analysis to maximize the number of axes within the band for the real data, we find that 13 axes are included. The probability of a value this large, assuming that $\mathscr{H}_\circ$ is true, is apparently very small.

Evidence that the concentration has *persisted* can be inferred when we note that for the 17th Catalogue data the simulations estimate that in only 4 of 10^4 cases would we find as many as 20 major axes in the band if in fact the null hypothesis was correct. Repeating the analysis to maximize the number of axes within the band for the real data we now find that 22 axes are included.

4.2. Inferring the orbit orientation of the concentration

We now discuss the alternative to the null hypothesis, the *assumption* that there is a systematic cause oriented along a plane. In Appendix A we describe a maximum likelihood analysis to find estimators of the parameters for the orbital angles Ω, i, and the half-width Γ of the band under this assumption. For the 11th Catalogue data we find maximum likelihood estimators $\hat{\Gamma}_m = 0.164$, $\hat{\Omega}_m = 318°$, $\hat{i}_m = 95° \rightarrow \hat{\kappa}_m = 13$ (of 15) axes inside the band. The 17–11th Catalogue maximum likelihood solution gives $\hat{\Omega}_m = 321°$, $\hat{i}_m = 105° \rightarrow \hat{\kappa}_m = 11$ (of 20) axes inside a band of the same width.

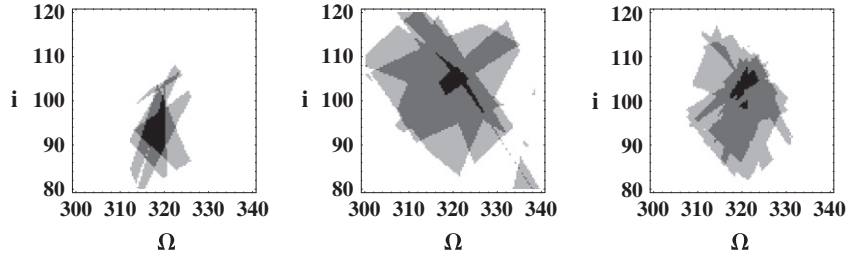

Fig. 6. Confidence regions of orientation angles (Ω = galactic longitude of ascending node, i = galactic inclination) of great circle bands (black – 68% confidence region, dark gray – 95% confidence region, light gray – 99% confidence region). (left) 11th Catalogue data. (middle) 17–11th Catalogue data. (right) 17th Catalogue data.

Table 1
Monte Carlo simulation distribution for Catalogue data set $\mathscr{E}$.

$\mathscr{E}$	n	κ	f_κ
11th	15	5	0.0004
		6	0.1141
		7	0.4768
		8	0.3056
		9	0.0826
		10	0.0178
		11	0.0024
		12	0.0003
17–11th	20	7	0.0072
		8	0.2214
		9	0.4345
		10	0.2400
		11	0.0782
		12	0.0180
		13	0.0007
17th	35	11	0.0067
		12	0.1244
		13	0.3205
		14	0.3037
		15	0.1621
		16	0.0598
		17	0.0168
		18	0.0042
		19	0.0014
		20	0.0004

An alternative view of the persistence of the concentration is that the maximum likelihood directions $\hat{\mathbf{h}}_m$ for the 11th Catalogue and for the 17–11th Catalogue differ by $\approx 10°$. If two directions were randomly chosen in a hemisphere, this would happen by chance <2% of the time. When we analyze the full 17th Catalogue data we find a maximum likelihood solution with $\hat{\Gamma}_m = 0.180$, $\hat{\Omega}_m = 319°$, $\hat{i}_m = 103° \rightarrow \hat{\kappa}_m = 23$ (of 35) axes inside the band.

We determine confidence regions of the band orientation angles (Ω, i) for each of the three data sets $\mathscr{E}$ by fixing $\Gamma = \hat{\Gamma}_m$. Assuming the truth of the alternative hypothesis, the probability that we would find k of n axes inside the band is the binomial probability distribution $P(k; n, p)$. In Appendix A our estimator of the statistic p is given by the $\hat{p}_m \equiv \hat{\kappa}_m/n = (13/15,\ 11/20,\ 23/35)$ for each of the three data sets respectively. We then specify confidence levels $1-\alpha = (0.68, 0.95, 0.99)$ and determine the smallest integer solution, $\kappa(\alpha)$, to the inequality

$$1-\alpha > \sum_{k=\kappa(\alpha)}^{n} P(k; n, \hat{p}_m) \tag{7}$$

Solutions corresponding to confidence levels $1-\alpha = (0.68, 0.95, 0.99)$ are $\kappa(\alpha) = (12, 11, 10)$ for the 11th Catalogue, (10, 7, 6) for the 17–11th Catalogue, and (22, 18, 16) for the 17th Catalogue respectively. Confidence *regions* for Ω, i, are now determined since every potential band orientation has an associated number of major axes enclosed for the real data. Confidence regions are shown in Fig. 6 (for the 17–11th Catalogue only the confidence region associated with $1-\alpha = 0.68$ is completely shown). These observations only describe the confidence regions for the direction of $\hat{\mathbf{h}}$ *if we reject the null hypothesis in favor of the alternative.*

The maximum likelihood estimator of $\hat{\mathbf{h}}$ for the 17th Catalogue data is centered near $i = 103°$, $\Omega = 319°$ (or its opposite direction). In ecliptic coordinates the maximum likelihood great circle plane is specified by $i_e = 133°$, $\Omega_e = 190°$, or its opposite direction. In Appendix B we list the 17th Catalogue data for the 102 comets that constitute our complete set. For each comet we include the binding energy parameter, x, the tidal characteristic, S, the perihelion distance, q, and the galactic angular orbital elements B, L and α. The last column gives the magnitude of the angular separation of the cometary major axis from the maximum likelihood great circle plane, γ. Comets having angular separations within $\pm\gamma$ fall inside a band of solid angle $4\pi \sin\gamma$. Comets with year designation prior to 1995 constitute our 11th Catalogue data. Fig. 7 gives the cumulative distribution in $\sin\gamma$ for the 11th and 17th Catalogues.

If we assume that the there is a systematic cause to the asymmetry, we can estimate the size of the enhancement in the present data for new comets (91 comets with $x < 60$ in Appendix B) as follows. Although only 13 of 35 comets lie outside of the maximum likelihood ±9.6° band for our best fit, at a confidence level = 0.95 we have 17 of 35 outside the band. So, conservatively, we would expect ≈3 inside the band if there were no systematically enhanced component. The excess of ≈15–19 inside the band is ≈20% of the complementary number of 76–72 for the new comet data. The same number can be obtained by extrapolating back to zero the large $\sin\gamma$ portion of the cumulative curve in Fig. 7.

Using an approach that ignores the characteristic S, Murray (1999) has argued for a solar companion that is the source of an impulsed observed Oort cloud population with $40 \leqslant x \leqslant 100$ whose axes are concentrated along a great circle that is different from that found here. He found that *all* such comets in the 10th Cometary Catalogue had axes within a ±30° band. His point is essentially that all of these observed comets *must* have been injected into the discernable zone by an impulse of a bound companion. We have taken the 17th Catalogue data and considered all $(40 \leqslant x \leqslant 100)$ comets that also were included in Murray's paper which analyzed 10th Catalogue data. A fit to the original data is found to agree with Murray's result, a best fit companion orbit plane with a galactic inclination of $i = 37°$ and galactic ascending node of $\Omega = 175°$ that includes all 12 10th Catalogue axes within a band of ±30° which encloses 1/2 of the celestial sphere. When we repeat the fit with the same band orientation and width we find that 10 of 25 additional comets in the 17th Catalogue are enclosed. The concentration originally perceived is seen to have disappeared.

4.3. IR observational limits on the companion's mass and distance

The absence of detection in the IRAS and 2mass data bases place limits on the range of possible masses and present distances of the proposed companion. For relevant values the 2mass limits are not very restrictive. Assuming a J-band detection magnitude limit of 16 and theoretical models of a 4.5 Gyr old 2—10 M_J object (Burrows et al., 2003), we find that the mass would have to be greater than 7 (10) M_J and closer than 6000(25,000) AU for a possible 2mass identification.

For jovian masses, the strongest current limits on distance are found from the IRAS Point Source and Faint Source Catalogs. We have performed a non-parallax search of both IRAS catalogs using the VizieR Service (http://www.vizier.u-strasbg.fr/cgi-bin/VizieR). The search was based on the theoretical models of Burrows et al. (2003). Search criteria included rejection of previously identified point sources, a PSC 12 μm flux greater than 1 Jy and a FSC flux greater than 0.3 Jy. The latter value is based on a completion limit of 100% (Moshir et al., 1992). Only flux quality class 1 sources were included. We further required that there be no bright optical or 2mass candidates within the 4σ error limits and that the absolute value of the galactic latitude be greater than 10°, as required for sources to appear in the FSC. Distant IR galaxies were excluded by requiring the 25 μm flux to be greater than the 60 μm flux. The PSC search yielded a single candidate, 07144 + 5206, with galactic coordinates $B = 25°$ and $L = 165°$, not far from the great circle band. The 12 and 25 μm band flux (0.8 Jy and 0.5 Jy) of this source is consistent with an ≈6 M_J mass at ≈6000 AU. However, the FSC, which is the definitive catalog for faint sources, associated this PSC source with another source located 80 arcsec away. This position corresponded to an extremely bright ($J = 6$) 2mass source. The negative IRAS search results suggest that an object of mass 2

(5) M_J must have a current distance $r \geqslant 2000(10{,}000)$ AU, respectively.

IRAS and 2mass observational constraints prohibit present locations $r < 2000{:}10{,}000{:}25{,}000$ AU for $M_p = 2{:}5{:}10\ M_J$ respectively. Dynamical constraints previously discussed suggest a maximum companion mass in the range $M_p \approx 1$–$4\ M_J$ and semimajor axis in the range $a \approx 30{,}000$–$10{,}000$ AU, respectively. Qualitatively the probability that there exists a companion with these appropriate parameters is the ratio of the specified companion parameter space area (M_p, a) to the complementary, non-IRAS(2mass)-excluded parameter space area. Next we try to roughly estimate this from the non-Catalogue evidence.

We assume that there is a certainty that the Sun has an as-yet-to-be-discovered maximum mass companion with mass between $M_{Pluto} \leftrightarrow 20\ M_J$, the upper limit being fixed by IRAS/2mass observations. What we seek to model is the distribution of the maximum wide-binary companion mass (within these limits) for a collection of solar-type stars. Zuckerman and Song (2009) give a mass distribution for brown dwarfs down to 13 M_J of $dN/dM \propto M^{-1.2}$. It might be assumed that this power law roughly holds down to the minimum Jeans mass limit of 1–4 M_J (Whitworth and Stamatellos, 2006) but the mass distribution below 1 M_J is completely unknown. For simplicity we assume that the distribution of maximum masses is $dN/dM \propto M^{-1}$ over the entire mass range.

Next we estimate the probability distribution in semimajor axis for this companion, assumed to be in the interval $10^2 \leftrightarrow 10^5$ AU, again subject to the IRAS(2mass) limits. We base this estimate on the known distribution of semimajor axes of wide binary stars. At least 2/3 of solar-type stars in the field reside in binary or multiple star systems (Duquennoy and Mayor, 1991). The fraction of these systems which have semimajor axes $a \geqslant 1000$ AU (wide binaries) is ≈15% (Kouwenhoven et al., 2010; Duquennoy and Mayor, 1991), and includes periods up to 30 Myr. The origin of these wide binaries may be capture during birth cluster dissolution (Kouwenhoven et al., 2010; Levison et al., 2010). For large semimajor axes the observed distribution is well approximated by $(dN/da) \propto a^{-1}$ and we adopt this power law for all maximum masses over the entire interval of a.

The simplifying assumptions we have made are equivalent to assuming a uniform probability distribution over the entire parameter space for the maximum mass companion under consideration

$$\frac{d^2N}{d\log M d\log a} = \text{constant}.$$

Thus the combined probability that the Sun has a companion of maximum mass 1–4 M_J with semimajor axis 30,000–10,000 AU is simply the ratio of this parameter area to the entire area after the IRAS constraint has been imposed. This value (≈0.015) crudely estimates the probability that a jovian mass companion resides in the inferred parameter space. If one believed that the maximum mass of an as yet to be discovered object must exceed Neptune's mass the probability estimate would change to ≈0.05.

4.4. Dynamical inferences of other perturber properties

Although the orbit normal of the putative companion is tightly constrained, other properties are less so. The near-uniform distribution of the overpopulation around the great circle suggests that it has a present orbit that is more nearly circular than parabolic $(e_p^2 < 0.5)$. The near-circular implication cannot remain true over the Solar System lifetime since the eccentricity and inclination osculate significantly due to the tide. Further, the semimajor axis will be affected by stellar impulses over these timescales.

The implication that $e_p^2 < 0.5$, is in fact, consistent with the present galactic inclination of the perturber inferred here, $i \approx 103°$. This follows from the near-conservation of the $\hat{\mathbf{z}}$ component of galactic angular momentum of objects in the IOC and OOC in the intervals between strong stellar impulses, $h_z \propto b\cos i \propto a\sqrt{1-e_p^2}\cos i \approx$ constant. Since the present value of $|\cos 103°| \approx 0.22$ is at the low end of a random distribution, $0 \leqslant |\cos i| \leqslant 1$, a larger primordial value of $|\cos i|$ implies that the present value of e_p is reduced from its primordial value.

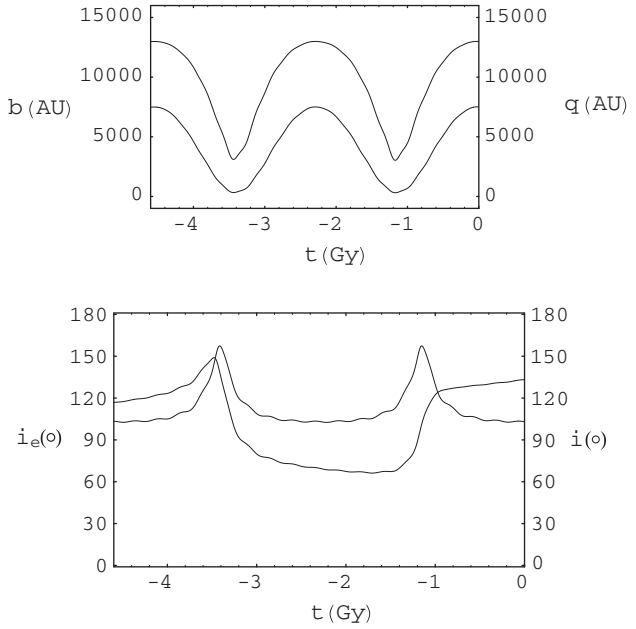

Fig. 8. Integrating back in time for 4.5 Gyr the osculating orbit of a conjectured companion with *present* ($t_o \equiv 0$) galactic orbital elements $i(0) = 103°$, $\Omega(0) = 319°$, $\omega(0) = 0$, $a = 15{,}000$ AU, $e_p(0) = 0.5$, $q(0) = 7500$ AU assuming unchanging galactic environment and neglecting impulsive perturbations. Shown are the perihelion distance, $q(t)$, and the semiminor axis, $b(t)$, along with the galactic and ecliptic inclinations, $i(t)$ and $i_e(t)$.

In Fig. 8 we show a representative time dependent companion orbit assuming present galactic orbital elements $i = 103°$, $\Omega = 319°$, $\omega = 0$, $a = 15{,}000$ AU and $e_p = 0.5$. We integrate back in time assuming an unchanging galactic environment and neglecting impulsive perturbations, both of which cannot be ignored for more reliable results. The purpose of the calculation is to demonstrate that significant changes in the eccentricity and inclination occur over the Solar System lifetime for a companion with $a > 10^4$ AU.

Setting the critical perturbation for $\gamma = 9.6°$ equal to the minimum change required to enter the discernable zone, Eq. (5) yields

$$|\Delta\mathbf{H}_{\mathbf{pert}}|_{\mathbf{crit}} = \sqrt{\mu_\odot a}\frac{\mu_p}{\mu_\odot}|\hat{\mathbf{Q}} \times \mathbf{I}|_{\mathbf{crit}} \equiv |\Delta\mathbf{H}_{\min}| \approx \sqrt{\mu_\odot 5.4\ \text{AU}}. \tag{8}$$

This provides a means of estimating the perturber properties needed to weakly impulse the OOC comet population and assist the tide in making a comet of semimajor axis $30 < x < 60$ discernable. Here $|\hat{\mathbf{Q}} \times \mathbf{I}|_{\mathbf{crit}}$ is taken to be $\simeq$ the peak values of $|\hat{\mathbf{Q}} \times \mathbf{I}|$ sampled over all orientations of $\hat{\mathbf{Q}}$ that are inclined to the great circle by an angle $\gamma = 9.6°$

$$\frac{M_p}{M_\odot}\sqrt{\frac{a}{5.4\ \text{AU}}}|\hat{\mathbf{Q}} \times \mathbf{I}|_{\mathbf{crit}} = 1. \tag{9}$$

In Fig. 9 we show an illustrative plot of $|\hat{\mathbf{Q}} \times \mathbf{I}|$ for perturber parameters $a = 15{,}000$ AU, $e_p = 0.5$, $f_o = 215°$ and comet $A = 22{,}000$ AU. A set of major axis orientations, $\hat{\mathbf{Q}}$, are considered which are all inclined along a conical surface at an angle $\gamma = 9.6°$ to the perturber plane. The specific orientation $\sigma = 180°$ corresponds to the case where $\hat{\mathbf{Q}}$ is closest to the perturber aphelion direction. The arbi-

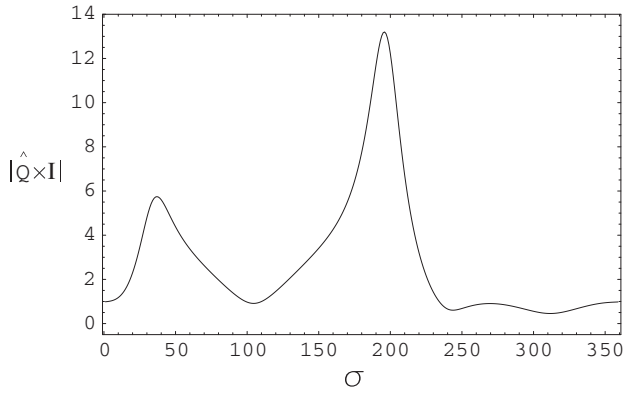

Fig. 9. An example case showing the single-orbit impulse strength $|\hat{\mathbf{Q}} \times \mathbf{I}|$ for comets with $A = 22{,}000$ AU and $\hat{\mathbf{Q}}$ inclined to the perturber plane by $\gamma = 9.6°$. The positions $\sigma = 0(180°)$ correspond to comet major axis orientations closest to the perturber perihelion (aphelion). Perturber parameters are $a = 15{,}000$ AU, $e_p = 0.5$, and $f_o = 215°$, the present true anomaly of the perturber.

trarily chosen *present* location of the companion is $f_o = 215°$ so that it has recently passed aphelion. Two peaks are shown corresponding to the two comet axes $\hat{\mathbf{Q}}$ that are most strongly impulsed on the way out and on the way in during the *prior* cometary orbit. The peak at $\sigma = 195°$ locates the perturber position when comets were impulsed on their inward leg. The ratio of the comet/perturber periods is ≈1.8 in this case and the second peak at $\sigma = 35°$, corresponds to the outward leg when the perturber was on its previous orbit. The importance of the reflex term can be gauged from the background contribution. The reflex contribution depends only moderately on $\hat{\mathbf{Q}}$. In general the peak corresponding to the inward comet leg will slightly lag the present perturber position if the perturber is presently more nearly at aphelion. The second peak corresponding to the outward leg will, in general, tend to be randomly positioned relative to the inward peak if $A > a$. Each peak contains comet axes $\hat{\mathbf{Q}}$ that may have had angular momentum impulses both aiding the tide and opposing the tide.

The results shown are typical for all $e_p < 0.5$, $90° < f_o < 270°$ when $10{,}000 \text{ AU} < a < 30{,}000$ AU. The exceptions include the less likely cases when the perturbations on both the outward and inward legs of a comet orbit find the perturber at the same general location $f \approx \sigma$ creating a larger net impulse. We shall adopt a typical value of $|\hat{\mathbf{Q}} \times \mathbf{I}|_{\mathbf{crit}} \approx 6\text{–}12$ for all possible orbit parameters above. Smaller values in this range typically occur for smaller values of a which have higher relative velocities at orbit crossing. Another aspect of the variation is that the smaller reflex term can add or subtract from the direct impulse term.

Inserting $M_p = 5$ M_J into Eq. (9) we obtain $a \approx 6000$ AU. Assuming $e_p^2 < 0.5$, this is marginally inconsistent with IRAS observational limits. Smaller masses should not conflict with IRAS. Thus we adopt an approximate range of perturber parameters $1\ M_J < M_p < 2\ M_J$ for $a \approx 30{,}000$ AU extending to $2\ M_J < M_p < 4\ M_J$ for $a \approx 10{,}000$ AU. This companion mass range is consistent with the minimum Jeans mass (1–7) M_J as variously calculated (Whitworth and Stamatellos, 2006; Low and Lynden-Bell, 1976), although cluster capture of ejected planets may be more likely (Kouwenhoven et al., 2010; Levison et al., 2010).

A solar companion remains a viable option (Matese et al., 1999; Horner and Evans, 2002). In addition, we find that an ≈4 M_J companion in an orbit such as that shown in Fig. 8 would be capable of adiabatically detaching a scattered disk EKBO, producing an object with orbital characteristics similar to Sedna (Matese et al., 2006; Gomes et al., 2006). Allowing for the possibility that the perturber was more tightly bound primordially, smaller masses are then allowed. It may also be possible to explain the misalignment of the invariable plane with the solar spin axis (Gomes et al., 2006) if the putative companion was more tightly bound primordially. Such a companion would have a temperature of ≈200 K (Burrows et al., 2003) and its infrared signature would have been recorded by the recently completed Wide-field Infrared Survey Explorer (WISE) mission.

Matese and Lissauer (2002) investigated the frequency of weak stellar showers as well as the patterns of new comet orbital elements. They found that stellar showers that produce a ⩾20% *peak* enhancement in the background tidal flux occur with a frequency of approximately once every 15 Myr. The half-maximum duration is ≈2 Myr. Thus it is only moderately unlikely that we are presently in a weak stellar shower of this magnitude. Flux enhancements of this magnitude were found to extend over an angular arc ≈150° and have a full-width half-max of ≈50°. Weak stellar impulses never extend over a larger arc. More simply put, to get the same stellar-induced flux enhancement as inferred from the data here, the enhanced region will have an extent that is ≈half as long and ≈twice as wide as that observed. Of course one must consider the possible alignment of two weaker coincident stellar impulses (or a single weaker statistical anomaly and a coincident single weaker stellar impulse) that happen to line up on opposite hemispheres. These will be improbable. For example, suppose we assume that there will always be two weak stellar impulses enhancing the observed background tidal flux, each with half the observed enhancement. The probability that both stellar orbit planes will be aligned to within ±9.6° is 0.014.

4.5. The absence of an impulsive component in other data

Young comets have been defined here as observed IOC comets with $60 \leqslant x \leqslant 1000$. The 17th Catalogue lists 64 young comets, 49 of which have $S = -1$, 15 of which have $S = +1$, a ratio that exceeds that of new comets (56 for $S = -1$, 35 for $S = +1$). Further, 13 young comets have future orbits that are unbound, 4 become bound new comets, 38 return to the young population and 9 become more tightly bound. Of the 91 observed new comets 50 have future orbits that are unbound, 8 return to the bound new population and 33 become young comets. None become more tightly bound than young comets. To complete the overview, the median perihelion distance for $S = -1$ young comets is ≈2.8 AU, while that for the $S = +1$ young comets is ≈2.7 AU. The corresponding results are ≈3.8 AU for the 56 $S = -1$ new comets and ≈2.5 AU for the 35 $S = +1$ new comets. There is *no evidence* of an overpopulation of $S = -1$ young comets (or of lower quality classes of new comets) within the perceived band. These observations require further discussion.

4.5.1. Young comets

Only 7 of 49 young comets with $S = -1$ are in the band – the band is underpopulated with young comets. The scatter in aphelion directions of these young comets is shown in Fig. 10. One observes a modest selection effect in which young comet aphelia are deficient in the equatorial north hemisphere, with polar direction located at galactic coordinates $L = 123°$, $B = 27°$. Young comets are less likely to be discovered if their perihelia are in the equatorial south hemisphere.

Any mechanism which is invoked for producing young comets should be able to explain the data which indicates that young comets preferentially have $S = -1$ to a degree that may exceed that of new comets. Three possible dynamical mechanisms for producing young comets include.

(i) An IOC comet with perihelion outside the loss cylinder weakly impulsed on its present orbit by a bound perturber such that it became a discernable young comet. These comets would preferentially have their major axes inside the

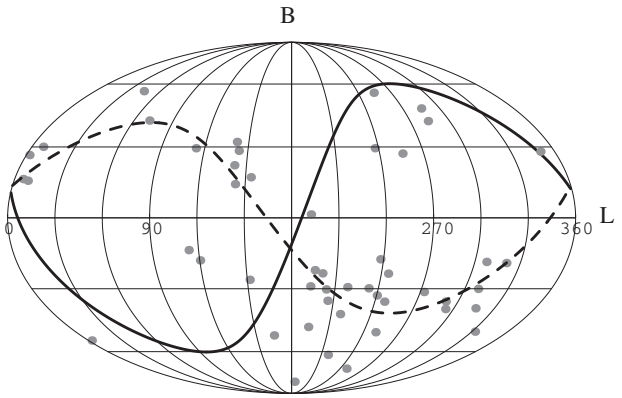

Fig. 10. The scatter distribution for aphelia directions of 17th Catalogue young comets having a binding energy parameter, $x \equiv 10^6\,\mathrm{AU}/A$, in the interval $60 \leqslant x \leqslant 1000$ and tidal characteristic $S = -1$. Solid curve: ecliptic plane. Dashed curve: maximum likelihood plane.

band and would exhibit the $S = -1$ preference since it is easier to move into the discernable zone from the $S = -1$ side than from the $S = +1$ side (see Fig. 1).

(ii) A new OOC comet impulsed in energy by the planets on its prior passage interior to the loss cylinder and converted into a present discernable young comet, sometimes referred to as a (young) daughter comet. In the absence of distinctive selection effects, such comets would preferentially maintain an imprint of the distribution of major axes of new comets. If the putative companion exists, they would then have an excess of their major axes inside the band and would preferentially have a $S = \mp 1$ ratio similar to the *complete* new comet population with $x < 60$.

(iii) An IOC comet whose perihelion has migrated from the outside to the inside of the loss cylinder due to the reflex motion of the sun induced by the perturber. Its energy would be changed by the planets on each passage and eventually it may become a young comet. Such comets would *not* be concentrated along the great circle, but would exhibit the $S = -1$ preference since it is easier to migrate into the discernable zone from the $S = -1$ side than from the $S = +1$ side.

The absence of an excess of young $S = -1$ comets inside the band requires that possible explanations for not producing populations (i) and (ii) be given.

First we discuss mechanism (i). For a comet major axis inclined to the perturber orbit plane by an angle γ, the angular momentum impulse $|\Delta\mathbf{H}_{\mathbf{pert}}|_{\mathbf{max}}$ varies approximately as $1/(V_{rel}\gamma)$, where V_{rel} is the relative velocity. The cross section for scattering comets varies approximately as γ^2 so that the requirements of a larger impulse to make IOC comets discernable, along with a larger relative velocity, imply a smaller γ. Thus one expects that a perturber in a crossing orbit with IOC comets would produce a narrower band of young comets perturbed with $|\Delta\mathbf{H}_{\mathbf{pert}}| > |\Delta\mathbf{H}_{\mathbf{min}}|$. The absence of any sign of such a directly impulsed population (i) in the perceived band is not inconsistent with the notion that the perturber induced depletion rate of this *in situ* IOC population with major axes within the great circle band would be larger than the rate of refilling of the IOC band phase space by the galactic tide or stellar impulses. But this remains to be demonstrated.

An instructive exercise is to apply the analysis of Appendix A and Section 4.1 to see if there is suggestive evidence of a directly impulsed population (i) in a *different* band. We determine the maximum likelihood orbit normal locating the plane of concentration of the young comet major axes shown in Fig. 10. When we do so we find that the maximum likelihood for (Ω, i) is associated with $\hat{\kappa}_m = 27$ and find that $\kappa(\alpha) = (25, 21, 19)$ at confidence levels $1 - \alpha = (0.68, 0.95, 0.99)$. The concentration inside this band is well distributed along the entire energy interval $60 \leqslant x \leqslant 1000$, therefore the hypothesis (i) of a bound perturber directly impulsing IOC comets would require that the perturber orbit have a perihelion distance $\leqslant$2000 AU. As before, when we perform a Monte Carlo simulation and randomize L for the 49 comets we find an unconstrained band which maximizes the number of major axes contained in the band and determine the frequency distribution f_κ. At confidence levels equal to that discussed for the 17th Catalogue 1A new comet data, f_κ is $\approx 8\times$ larger.

More difficult to explain than the absence of an enhanced young population (i) in the perceived band is the absence of a young daughter population (ii). It is commonly argued that young comets are predominantly produced by this dynamical path. To explain the relative numbers of long-period comets, fading is invoked. In one model approximately 95% of dynamically produced daughters survive for roughly 6 orbits and the remainder do not fade (Wiegert and Tremaine, 1999). However, they observe that "Although physically plausible, fading remains an *ad hoc* explanation for the distribution of LP comet orbits which has not been independently confirmed, and we should remain alert for other possible explanations."

The fraction of $S = -1$ comets for the young population (49/64) is somewhat difficult to reconcile with the corresponding number for the new population (56/91) if we assume that the $S \mp 1$ ratio is the same for both populations as one might expect if both $S = \mp 1$ new comets are equally likely to give rise to daughters. The statistical estimates for the probability of a comet having $S = -1$ (and the corresponding standard error) is $p_{est} \pm \sigma(p_{est}) = 0.766 \pm 0.053$ for the young population and 0.615 ± 0.051 for the new population. A selection effect might be invoked, but the larger median q for new comets as compared to young comets works in the wrong direction; larger q correlates with weaker perturbations which then correlates with a *greater* likelihood for $S = -1$. We then conclude that the most likely way the Tyche conjecture could be invoked to explain the great circle band excess in the new population, and be consistent with the corresponding absence of an excess in the young population, is to postulate that nearly all daughter comets fade more rapidly than is presently assumed.

This in turn drives us to suggest an alternative dynamical mechanism for producing young comets, (iii) the migration of IOC comets into the discernable zone induced by the solar reflex motion. Since the shortest phase space path from outside the loss cylinder to the interior of the discernable zone is from the $S = -1$ direction, we can expect that a preponderance of $S = -1$ young comets will result from this mechanism. Note that in this dynamical mechanism the galactic tide prepares the IOC phase space external to the loss cylinder while the solar reflex motion due to the perturber is predominantly responsible for making these comets enter the discernable zone. This mechanism acts more efficiently on IOC comets if the semimajor axis of the conjectured companion is more nearly at the lower limit allowed by IRAS. A direct numerical integration including a companion, of the type done by Kaib and Quinn (2009), is needed to clarify the viability of this speculation. If Tyche exists, the *in situ* population of the IOC and OOC will be significantly altered from that obtained in other models.

4.5.2. Class 1B new comets

Class 1B new comets ($-\infty < x < 60$) also have the characteristic galactic signature as there are 30 comets with $S = -1$ and only 13 with $S = +1$, a ratio intermediate to that of class 1A new and young comets. As described above, a search for a weak impulsive signature should be confined to the $S = -1$ new comet data. We find that the $S = -1$ dominance for 1B new comets no longer correlates with the energy range $30 < x < 60$. This is interpretable as evidence of er-

rors in the determination of x for this quality class, as previously discussed. A clearer picture of the true uncertainty, including unmodelled outgassing effects, is suggested by the observations that only 2 of the 56 $S=-1$ class 1A new comets are nominally unbound, while 11 of the 30 $S=-1$ class 1B new comets are nominally unbound. Further evidence that outgassing is more important for class 1B new comets is the fact that the median perihelion distance of the $S=-1$ class 1B new comets is 1.5 AU, while that of the $S=-1$ class 1A new comets is 3.8 AU. These observations suggest that the 1B new comet population may be much more contaminated by truly young comets because of outgassing energy errors than is the class 1A new comet population.

When we do a maximum likelihood search for the orbit normal $\hat{\mathbf{h}}$ using the same procedure described in Appendix A with the evidence being the 30 $S=-1$ class 1B new comet major axes, the maximum likelihood orientation has $\hat{\kappa}_m = 14$ axes falling within the band, but again the band orientation is well removed from that found for class 1A new comets. A confidence level of 0.99 is associated with $\kappa(\alpha)=8$, extends over a large solid angle, and has an insignificant P-value. The maximum likelihood band orientation obtained for the $30<x<60$ class 1A evidence does include 8 of these 30 axes.

A selection effect that partially explains the different levels of enhancement in the class 1A and 1B evidence is as follows: Class 1A new comets have less outgassing $\leftrightarrow$ larger perihelion distances. But larger perihelion distances correlate with weak perturbations, those that are most likely to exhibit the effect of a bound perturber. Therefore class 1A evidence preferentially selects weak perturbations.

5. Summary and conclusions

We have described how the dynamics of a dominant galactic tidal interaction, weakly aided by an impulsive perturbation, predicts specific properties for distributions of galactic orbital elements of observed outer Oort cloud comets. These subtle predictions have been found to be manifest in high-quality observational data, suggesting that the observed OOC comet population contains an anomalous excess of ≈20% oriented along a well-defined arc. The extent of the enhanced arc is inconsistent with a weak stellar impulse, but is consistent with a jovian mass solar companion orbiting in the Oort cloud. A putative companion with these properties may also be capable of producing detached Kuiper Belt objects such as Sedna and has been given the name Tyche. Tyche would have depleted the inner Oort cloud over the Solar System lifetime requiring a corresponding increase in the inferred primordial Oort cloud population. A substantive difficulty with the Tyche conjecture is the absence of a corresponding impulsively produced excess in the observed IOC comet population.

Acknowledgments

The authors thank Jack J. Lissauer for his continuing interest and for his contributions to this research. Additionally, useful referee comments were provided by Julio Fernandez. We also acknowledge the guidance in statistical matters that has been provided by Charles L. Anderson.

Appendix A. Maximum likelihood analysis for the orbit plane orientation.

The relevant parameters of the putative companion are e_p, M_p, a, Ω, i. In Sections 4.3 and 4.4 we discuss the rationale for estimating the allowed ranges of values for e_p, M_p, a and these can loosely be taken as the 1σ confidence intervals. Here we discuss the more restrictive limits on orbital parameters, those inferred from a likelihood analysis involving the orbit plane orientation angles Ω, i associated with the orbit plane normal $\hat{\mathbf{h}}$. The evidence under consideration is composed of the set of major axis orientations, $\mathscr{E} = \hat{\mathbf{Q}}_j, (j=1,n)$. Let $z_j \equiv \mid \hat{\mathbf{Q}}_j \cdot \hat{\mathbf{h}} \mid \equiv \sin\gamma_j$, a measure of the misalignment of the jth comet major axis with the assumed plane. Note that z_j implicitly depends on the unknown orbital parameters Ω, i. Our goal is to determine a maximal measure of the degree of concentration of these axes along the unknown plane. In Fig. 7 we show the cumulative number distribution of major axes for a specific choice of $\hat{\mathbf{h}}$, $n(\leqslant \sin\gamma; \hat{\mathbf{h}})$.

The probability density function describing the likelihood of measuring z_j given p, Ω, i, Γ is defined as1

$$f(\mathscr{E}|p,\Omega,i,\Gamma) \equiv \begin{cases} \frac{p}{\Gamma} & \Gamma \geqslant z_j \geqslant 0, \\ \frac{1-p}{1-\Gamma} & 1 \geqslant z_j > \Gamma, \end{cases}$$

where $0<p<1$, Ω, i, Γ are free parameters whose values are to be determined by maximizing the likelihood function

$$\mathscr{L}(p,\Omega,i,\Gamma|\mathscr{E}) \equiv \prod_{j=1}^{n} f(\mathscr{E}|p,\Omega,i,\Gamma) = \left(\frac{p}{\Gamma}\right)^{\kappa}\left(\frac{1-p}{1-\Gamma}\right)^{n-\kappa}.$$

Here $\kappa \equiv n(\leqslant \Gamma; \hat{\mathbf{h}}) \leqslant n$ is the number of axes inside the band of halfwidth Γ having orientation angles Ω, i.

The maximum likelihood estimator of the parameter p (for arbitrary Ω, i, Γ) is then κ/n such that

$$\mathscr{L}(p\to\kappa/n,\Omega,i,\Gamma|\mathscr{E}) = \left(\frac{\kappa/n}{\Gamma}\right)^{\kappa}\left(\frac{1-\kappa/n}{1-\Gamma}\right)^{n-\kappa}.$$

A maximum in the likelihood function is expected to occur in the vicinity of the parameter estimators $\hat{\Gamma}_m \approx 1/6$, $\hat{\Omega}_m \approx 315^\circ$, $\hat{i}_m \approx 90^\circ$ based on Fig. 4 and prior work (Matese et al., 1999). To find the maximum likelihood for $\mathscr{E} = 11$th we scan this vicinity and maximize the likelihood when the parameters take on the values $\hat{\Gamma}_m = 0.164,\ \hat{\Omega}_m = 318^\circ,\ \hat{i}_m = 95^\circ \to \hat{\kappa}_m = 13, \hat{p}_m = 13/15$.

Table 2
Appendix B: Orbital elements of all 17th Catalogue class 1A comets with $x<100$. All angles are in degrees.

Comet name	x	S	q (AU)	B	L	α	γ
C/1996 J1-A (J1-B)	−510 (−1)	−1	1.2978	15.9	202.6	55.0	51.13
C/1996 E1	−42	1	1.3590	−22.6	304.3	319.2	18.39
C/1942 C2	−34	1	4.1134	−24.5	18.8	335.2	42.27
C/1946 C1	−13	1	1.7241	−60.3	313.1	276.7	14.17
C/2005 B1	−13	1	3.2049	−17.6	282.6	12.7	38.28
C/1946 U1	−1	1	2.4077	49.0	347.2	255.0	28.13
C/1997 BA6	0	−1	3.4364	27.7	123.0	52.9	20.05
C/1993 Q1	3	1	0.9673	41.2	112.7	174.6	28.22
C/2005 K1	7	1	3.6929	−17.3	227.4	312.1	85.45
C/2003 T3	10	1	1.4811	25.5	293.6	148.9	16.25
C/2006 L2	10	−1	1.9939	−50.0	225.1	98.2	52.89
C/1974 V1	11	−1	6.0189	28.0	308.9	63.1	2.61
C/1988 B1	13	−1	5.0308	−47.6	316.3	122.1	11.37
C/2006 K1	13	1	4.4255	66.1	56.2	247.3	36.69
C/2004 X3	14	1	4.4023	−36.8	80.9	24.1	31.90
C/2005 E2	14	1	1.5196	42.0	312.6	134.6	3.99
C/2006 OF2	15	1	2.4314	10.5	322.5	133.0	5.75
C/1991 F2	16	−1	1.5177	29.7	90.0	345.1	48.65
C/2005 G1	16	−1	4.9607	−55.3	297.9	100.6	22.60
C/1916 G1	17	−1	1.6864	17.9	225.9	30.1	58.95
C/1956 F1-A	17	1	4.4473	−25.4	180.0	62.1	42.33
C/1944 K2	18	−1	2.2259	−31.8	124.3	159.3	5.25
C/2007 O1	18	−1	2.8767	2.1	197.3	7.6	55.06
C/1935 Q1	19	1	4.0434	11.8	248.0	115.3	58.81
C/1999 J2	19	−1	7.1098	−49.9	234.4	259.3	52.80

Table 2 (*continued*)

Comet name	x	S	q (AU)	B	L	α	γ
C/1973 E1	20	−1	0.1424	17.0	207.3	46.3	53.15
C/1984 W2	20	1	4.0002	33.1	79.5	101.0	55.69
C/2001 C1	20	1	5.1046	−8.3	135.0	344.1	2.02
C/2004 P1	20	−1	6.0141	20.2	208.7	63.7	51.26
C/1922 U1	21	−1	2.2588	16.3	270.6	52.4	39.46
C/1997 A1	21	1	3.1572	−19.9	352.3	306.7	25.22
C/2003 K4	23	1	1.0236	−46.8	104.3	307.2	12.49
C/2005 Q1	23	−1	6.4084	−8.8	321.7	258.1	0.65
C/1947 S1	24	1	0.7481	10.9	185.4	170.2	40.61
C/1978 H1	24	1	1.1365	−20.7	124.4	30.2	8.65
C/1999 K5	24	−1	3.2554	34.1	129.8	271.8	14.81
C/2001 G1	24	−1	8.2356	−46.8	113.6	118.9	7.02
C/2006 HW51	25	1	2.2656	−35.4	162.3	83.4	26.39
C/1914 M1	27	−1	3.7468	−1.4	200.9	100.9	59.81
C/1980 E1	27	1	3.3639	−18.2	177.0	29.9	39.78
C/2004 YJ35	27	−1	1.7812	−38.2	346.3	122.2	12.23
C/1992 J1	28	1	3.0070	−43.8	316.9	0.3	10.47
C/1913 Y1	29	−1	1.1045	−52.4	283.0	237.4	31.83
C/1987 W3	29	−1	3.3328	64.7	333.5	62.5	17.92
C/2001 K5	29	1	5.1843	−30.3	223.1	78.8	71.80
C/1989 X1	32	−1	0.3498	−41.0	325.6	218.0	3.57
C/1978 A1	33	−1	5.6064	−31.4	142.3	167.8	9.48
C/1993 K1	33	−1	4.8493	2.3	130.9	347.4	8.38
C/1948 E1	34	1	2.1071	−38.6	250.2	83.2	58.25
C/1948 T1	34	−1	3.2611	17.9	324.0	306.9	8.63
C/2006 Q1	34	−1	2.7636	−45.5	112.2	134.0	8.48
C/1925 F1	35	1	4.1808	−40.9	65.6	327.8	33.96
C/2002 J4	35	−1	3.6338	32.4	162.6	342.6	12.07
C/1974 F1	36	−1	3.0115	21.7	140.3	10.7	3.59
C/2003 S3	36	−1	8.1294	11.6	345.3	351.9	27.95
C/2004 B1	36	1	1.6019	27.7	167.1	138.4	17.55
C/1950 K1	37	−1	2.5723	−43.8	137.7	269.9	8.02
C/1999 U4	37	−1	4.9153	−30.2	322.6	183.8	3.42
C/2006 E1	37	−1	6.0406	31.4	140.5	290.6	21.24
C/2006 P1	37	1	0.1707	−5.0	342.2	72.9	5.47
C/1999 F1	38	−1	5.7869	15.2	99.7	341.0	68.86
C/1999 U1	38	−1	4.1376	25.1	67.4	291.1	40.91
C/2000 CT54	38	−1	3.1561	36.7	145.1	8.0	2.96
C/2002 L9	38	−1	7.0330	51.6	147.6	292.5	4.93
C/1954 Y1	39	−1	4.0769	−23.5	314.1	232.3	9.55
C/1925 G1	40	1	1.1095	10.5	238.3	151.2	64.77
C/1997 J2	40	1	3.0511	−0.5	261.1	332.6	55.83
C/1954 O2	42	1	3.8699	−18.4	336.4	53.3	11.82
C/1979 M3	42	1	4.6869	14.1	207.0	126.6	55.24
C/2000 K1	42	−1	6.2761	−21.6	190.7	144.5	52.50
C/2006 S3	42	−1	5.1309	−15.3	188.0	219.4	50.21
C/1946 P1	44	−1	1.1361	−20.0	126.6	108.7	6.85
C/1999 Y1	44	−1	3.0912	62.7	289.2	326.2	1.31
C/2000 A1	44	−1	9.7431	−33.0	19.7	171.9	36.22
C/2005 EL173	44	−1	3.8863	23.3	50.4	350.5	79.60
C/1932 M2	45	−1	2.3136	−14.6	146.5	172.1	10.33
C/1987 H1	46	−1	5.4575	−17.6	190.9	161.4	53.02
C/1888 R1	48	−1	1.8149	59.5	313.7	289.0	8.54
C/1983 O1	48	−1	3.3179	55.2	324.4	355.4	13.71
C/1973 A1	49	−1	2.5111	−50.7	106.2	220.9	9.24
C/1989 Y1	49	1	1.5692	−6.1	328.9	96.2	8.22
C/2007 D1	50	−1	8.7936	−41.3	64.4	157.8	33.83
C/2003 WT42	51	−1	5.1909	−56.8	353.7	171.0	6.59
C/2000 O1	52	−1	5.9217	23.5	313.8	286.2	25.23
C/2000 SV74	52	−1	3.5417	−21.5	296.7	193.5	0.53
C/1999 F2	54	−1	4.7188	−46.0	135.3	112.9	6.83
C/1999 S2	56	−1	6.4662	22.2	153.2	322.9	7.83
C/2006 K3	56	1	2.5015	46.6	22.7	261.9	49.79
C/1976 D2	59	1	6.8807	−44.5	120.9	315.8	3.36
C/1987 F1	59	−1	3.6246	−26.5	129.8	186.4	2.20
C/1993 F1	59	−1	5.9005	−45.0	330.2	213.7	1.44
C/2002 J5	60	−1	5.7268	−33.0	240.2	157.1	67.57
C/2005 L3	60	−1	5.5933	−30.3	203.9	169.6	61.07
C/2000 Y1	61	−1	7.9748	28.0	350.3	8.5	33.52
C/1999 H3	65	−1	3.5009	−50.1	250.1	167.3	49.12
C/1898 L1	68	−1	1.7016	28.3	143.8	315.4	2.01
C/1999 N4	68	−1	5.5047	−23.3	200.6	204.1	61.14
C/1972 L1	69	1	4.2757	−40.3	235.4	66.6	62.09
C/2007 JA21	69	−1	5.3682	−31.4	272.5	247.5	46.07
C/1958 R1	76	−1	1.6282	−18.4	307.6	133.4	14.74
C/1955 G1	82	−1	4.4957	−29.8	233.2	168.5	72.73
C/2005 A1-A	94	−1	0.9069	29.4	113.9	12.6	28.06

Now we repeat the above analysis for $\mathscr{E}$ = 17th. In a preliminary calculation, we fix $\Gamma = 1/6$, and find that the likelihood is maximized when $\Omega = 319°$, $i = 103° \rightarrow \kappa = 22$. This is the great circle fit shown in Fig. 5. A slightly larger maximum likelihood is found when we increase the halfwidth to $\hat{\Gamma}_m = 0.180 \rightarrow \hat{\kappa}_m = 23$, $\hat{p}_m = 23/35$ for the same direction of $\hat{\mathbf{h}}$. A separate question now is the maximum likelihood direction of the more recent evidence, $\mathscr{E}$ = 17–11th. Again we fix $\Gamma = 1/6$ and maximize the likelihood to find $\hat{\Omega}_m = 321°,\ \hat{i}_m = 105° \rightarrow \hat{\kappa}_m = 11,\ \hat{p}_m = 11/20$.

Concluding, we note that this analysis only yields maximum likelihood estimators for Γ, Ω, i, p under the *assumption* that the data requires a systematic cause oriented along a plane, the alternative to the null hypothesis discussed in Section 4.1.

Appendix B

See Table 2.

References

Burrows, A., Sudarsky, D., Lunine, J.J., 2003. Beyond the T dwarfs: Theoretical spectra, colors and detectability of the coolest brown dwarfs. Astrophys. J. 596, 587–596. <http://zenith.as.arizona.edu/~burrows/evolution3.html>.

Davis, P.Hut, Muller, R., 1984. Extinction of species by periodic comet showers. Nature 308, 715–717.

Delsemme, A.H., 1987. Galactic tides affect the Oort cloud: An observational confirmation. Astron. Astrophys. 187, 913–918.

Duquennoy, A., Mayor, M., 1991. Multiplicity among solar-type stars in the solar neighborhood: II. Distribution of the orbital elements in an unbiased sample. Astron. Astrophys. 248, 485–524.

Fernandez, J., 1981. New and evolved comets in the Solar System. Astron. Astrophys. 96, 26–35.

Gomes, R.S., Matese, J.J., Lissauer, J.J., 2006. A distant planetary-mass solar companion may have produced distant detached objects. Icarus 184, 589–601.

Heisler, J., Tremaine, S., 1986. Influence of the galactic tidal field on the Oort cloud. Icarus 65, 13–26.

Horner, J., Evans, N.W., 2002. Biases in cometary Catalogues and Planet X. Mon. Not. R. Astron. Soc. 335, 641–654.

Kaib, N.A., Quinn, T., 2009. Reassessing the source of long-period comets. Science 325, 1234–1236.

Kirpatrick, D., Wright, N., 2010. (Quoted in) Sun's Nemesis pelted Earth with comets, study suggests. <Space.com/scienceastronomy/nemesis-comets-earth-am-100311.html>.

Kouwenhoven, M.B.N., Goodwin, S.P., Parker, R.J., Davies, M.B., Malmberg, D., Kroupa P., 2010. The formation of very wide binaries during the star cluster dissolution phase. arXiv:1001.3969V1[astro-ph.GA]

Kresák, L., 1992. Are there any comets coming from interstellar space? Astron. Astrophys. 259, 682–691.

Królikowska, M., 2006. Non-gravitational effects in long-period comets and the size of the Oort cloud. Acta Astron. 56, 385–412.

Levison, H.F., Duncan, M.J., Brasser, R., Kaufman, D.E., 2010. Capture of the Sun's Oort cloud from stars in its birth cluster. Science 329, 187–190.

Low, C., Lynden-Bell, D., 1976. The minimum Jeans mass when fragmentation must stop. Mon. Not. R. Astron. Soc. 176, 367–390.

Marsden, B.G., Williams, G.V., 2008. Catalogue of Cometary Orbits, 17th ed. Smithsonian Astrophysical Observatory, Cambridge, MA.

Marsden, B.G., Sekanina, Z., Everhart, E., 1978. New osculating orbits for 110 comets and analysis of original orbits for 200 comets. Astron. J. 83, 64–71.

Matese, J.J., Lissauer, J.J., 2002. Characteristics and frequency of weak stellar impulses of the Oort cloud. Icarus 157, 228–240.

Matese, J.J., Lissauer, J.J., 2004. Perihelion evolution of observed new comets implies the dominance of the galactic tide in making Oort cloud comets observable. Icarus 170, 508–513.

Matese, J.J., Whitman, P.G., 1992. A model of the galactic tidal interaction with the Oort comet cloud. Celest. Mech. Dynam. Astron. 54, 13–36.

Matese, J.J., Whitman, P.G., Whitmire, D.P., 1999. Cometary evidence of a massive body in the outer Oort cloud. Icarus 141, 354–366.

Matese, J.J., Whitmire, D.P., Lissauer, J.J., 2006. A wide binary solar companion as a possible origin of Sedna-like objects. Earth Moon Planets 97, 459–470.

Moshir, M. et al., 1992. Explanatory Supplement to the IRAS Faint Source Survey version 2. JPL D-10015 8/92 (Pasadena:JPL), Figure III.C.1.

Murray, J.B., 1999. Arguments for the presence of a distant large undiscovered Solar System planet. Mon. Not. R. Astron. Soc. 309, 31–34.

Oort, J.H., 1950. The structure of the cloud of comets surrounding the Solar System, and a hypothesis concerning its structure. Bull. Astron. Inst. Neth. 11, 91–110.

Rickman, H.M., Fouchard, M., Froeschlé, C., Valsecchi, G.B., 2008. Injection of Oort cloud comets: The fundamental role of stellar perturbations. Celest. Mech. Dynam. Astron. 102, 111–132.

Whitmire, D., Jackson, A., 1984. Are periodic mass extinctions driven by a distant solar companion? Nature 308, 713–715.

Whitworth, A.P., Stamatellos, D., 2006. The minimum mass for star formation, and the origin of binary brown dwarfs. Astron. Astrophys. 458, 817–829.
Wiegert, P., Tremaine, S., 1999. The evolution of long-period comets. Icarus 137, 84–122.
Wright, E.L., 2007. Wide-field Infrared Survey Explorer. <http://www.astro.ucla.edu/~wright/WISE/index.html>.
Zheng, J.-Q., Valtonen, M.J., Valtaoja, L., 1990. Capture of comets during the evolution of a star cluster and the origin of the Oort cloud. Celest. Mech. Dynam. Astron. 49, 265–272.
Zuckerman, B., Song, I., 2009. The minimum Jeans mass, brown dwarf companion IMF and predictions for detection of Y-type dwarfs. Astron. Astrophys. 493, 1149–1154.